ЖЭТФ/JETP, 2026, том 169, вып. 3, стр. 306–313

ELECTRONIC STRUCTURE AND CHARGE TRANSFER IN THE κ-BEDT-TTF$_2$Cu$_2$(CN)$_3$ ORGANIC CONDUCTOR: THE ROLE OF Cu^{2+} IMPURITIES

A. V. Kuzmin**, E. I. Khasanova, S. S. Khasanov

Osipyan Institute of Solid State Physics
of the Russian Academy of Siences
142432, Chernogolovka, Moscow region, Russia

Received December 16, 2025,
revised version January 21, 2026
Accepted for publication January 26, 2026

The single crystals of the layered organic conductor κ-BEDT-TTF$_2$Cu$_2$(CN)$_3$ were studied by X-ray diffraction and X-ray photoemission spectroscopy. The electronic structure of the conducting BEDT-TTF$_2$ layer and its Fermi surface details were analyzed by quantum chemical calculations within the DFT level theory based on structure model of the isolated positively charged conducting layers in a virtual charge compensation medium. Although the accepted stoichiometry for the κ-salts corresponds to the half-filled band structure model with a charge transfer level of $q = 0.5$ for the dimers [BEDT-TTF$_2$]$^{2q+}$, it was found that, for the crystals studied, minimum of the corrections to the system's total energy reaches a minimum at $q = 0.488$. This theoretically found charge reduction in the cationic conducting layer is presumably associated with the presence of positively charged impurities within the anion layer. Indeed, X-ray photoemission spectroscopy measurements taken in this work clearly show the presence of Cu^{2+} impurities, which reduce the average negative charge of the anion layer and, consequently, the positive charge of the layer of cationic conducting dimers. The consequences of this result for the conducting properties of the crystal are also discussed.

Keywords: organic conductors, crystal structure, low temperatures, DFT

DOI: 10.7868/S3034641X26030055

1. INTRODUCTION

Since 1982, when G. Saito and co-authors [1] found the first metallic compound based on adjusted π-conjugated donor BEDT-TTF (ET) molecules [2] the interest in organic complexes with a quasi-2D electronic structure has been steadily growing. The κ-type $ET_2Cu_2(CN)_3$ or κ-CN salts with polymer-like inorganic anions $Cu_2(CN)_3$, studied by U. Geiser's group [3] in 1991, deserve great attention due to their superconducting properties and spin-frustration possibilities within the anisotropic triangular sublattice of the face-to-face pair of ET molecules [4–6]. Several studies analyzed the magnetic and optical behavior of these salts within a wide range of temperatures and pressures [7–9]. Despite a brief description of the structural issue, their results revealed an exotic phase transition diagram of κ-CN. It showed a Mott transition at $T \approx 25$ K (ambient pressure), [10, 11] a superconducting transition at ~ 3 K and a pressure higher than $P \approx 14 \cdot 10^4$ kPa [12, 13] and a probable spin-liquid state with no long-range magnetic ordering down to ~ 32 mK and an antiferromagnetic exchange interaction of ~ 250 K [4].

The group of authors proved and described the critical importance of structure-property relationships for all those peculiarities of κ-CN crystals [14]. In their comprehensive review, they explained that the unusual electronic interactions of κ-CN salts are mainly determined by features of the atomic structure such as details of the spatial arrangement of ET molecules, including intermolecular distances and their orientations relative to anionic layers. The latter aspects were elucidated in relatively recent works [5]. One of the most intriguing issues is the influence of the isolating anionic layer on the magnetic properties and conductiv-

* E-mail: kuzminav@issp.ac.ru

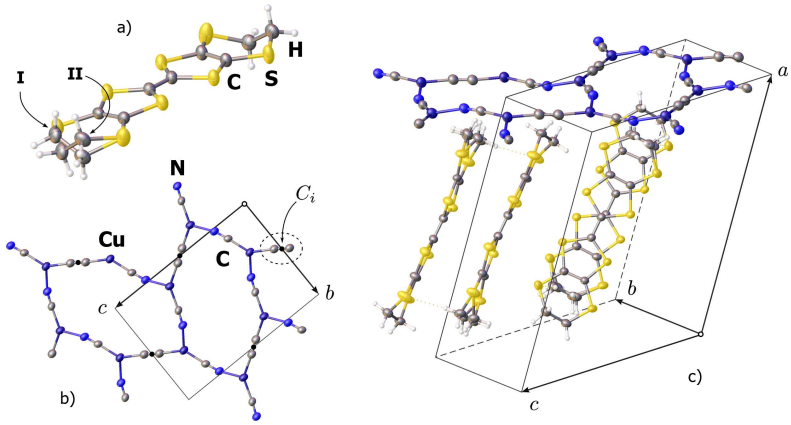

Fig. 1. Structure of κ-CN crystals: *a* — ET molecule with disordered $-C_2H_4-$ parts, *b* — anionic $Cu_2(CN)_3$ layer, *c* — layered crystal structure of κ-CN

ity of κ-CN crystals. For instance, violations of the inversion symmetry law at a position of $C \equiv N$ groups may be the reason for anomalous features in the dielectric constant and mean relaxation time that were observed using Hall effect measurements and dielectric spectroscopy [15]. At the same time, local breaks of $-C \equiv N-$ chains within cyano-polymer alter the optical properties of κ-CN crystals [16].

In order to find examples of this types of structure-property correlations, we studied the crystal structure at low temperatures and the X-ray photoemission spectra of our κ-CN samples. We found the traces of Cu^{2+} impurities in the anionic layers of our κ-CN crystals and proposed that they have an effect on the conductivity of the crystals.

2. EXPERIMENTAL

The κ-CN single crystals were obtained by electrocrytallizsation according to the method described in previous papers [17]. All well-shaped crystals were sorted by fast X-ray screening to select the most proper samples. These samples were used for a thorough X-ray diffraction analysis. For this purpose, we used our laboratory Rigaku-Oxford Diffraction Gemini R CCD diffractometer with a κ-type goniometer (Mo $K\alpha$ radiation).

XPS was performed using a Kratos Axis Ultra DLD spectrometer. The charge neutralizer with low-energy electrons was utilized to exclude the surface charging effects, and the binding energy of C 1*s* at 284.8 eV was used as the charge reference. The XPS data were analyzed using the Casa XPS software with the Gaussian/Lorentzian line shape and Shirley background correction. All XPS binding energies reported here have an uncertainty of ± 0.1 eV.

The calculations of the electronic structure were performed within the methods of density functional theory (DFT) using the Quantum Espresso (QE) software [18]. Monkhost-Pack *k*-point type grids with a size of $3 \times 7 \times 9$ and the SSSP Efficiency PBESol 1.1 pseudopotential library were taken. The calculations were based on the structural data obtained from the low-temperature X-ray diffraction experiments, and the atomic positions did not change during the calculation routines.

3. RESULTS AND DISCUSSION

3.1. Crystal structure

The structure of κ-CN crystals was investigated by X-ray diffraction analysis. The diffraction data were obtained in a temperature range of 100 to 300 K. The crystals had a perfect habit and a plate-like shape with typical sizes of $0.1 \times 0.3 \times 0.6\,\text{mm}^3$. The vast majority of them were twinned. The twinned crystals had no visible distinguishing features compared to the untwinned samples. Thus, only a preliminary X-ray study may help to separate one from another. However, in some cases we were able to split the crystals along the (100) plane and obtain two untwinned samples. One of them was used for the high-quality low-temperature X-ray structure analysis. The structure was solved by dual methods using SHELXT and refined by full-matrix least-squares methods against F^2 using SHELXL [19, 20]. All non-hydrogen atoms were refined with anisotropic displacement parameters. The hydrogen atoms were refined isotropically at calculated

positions using a riding model with their U_{iso} values constrained to 1.5 times the U_{eq} of their pivot atoms for terminal sp^3 carbon atoms and 1.2 times for all other carbon atoms.

The structure of κ-CN salts at room temperature was previously reported by U. Geiser [3]. The study of the temperature dependence of structure parameters was performed by H. Jeschke and co-authors [5]. Typically, κ-CN salt has a sandwich structure with alternating anionic isolating layers and conductive cationic layers (see Fig. 1c). At room temperature, it has the following crystallographic parameters: $a = 16.0635(4)$ Å, $b = 8.5586(2)$ Å, $c = 13.2582(3)$ Å, $\beta = 114.894(3)^\circ$, $V = 1653.40(8)$ Å^3, $Z = 1$, and space group $P2_1/c$; there are no abrupt changes in their temperature dependence up to 100 K.

The anionic layers consist of a 2D polymeric network that is formed by copper cations connected through cyanide CN anions (see Fig. 1b). There are inversion centers C_i in the copper cyanide polymer located at some C ≡ N groups. The inversion symmetry law led to the orientationally disordered of C ≡ N groups with half-occupied positions of carbon and nitrogen atoms. The possibility of local symmetry breakings in the layer was discussed by M. Pinterić and co-authors [15]. The individual building blocks of the cation layer act as pairs of face-to-face aligned ET molecules (see Fig. 1a), which are held together via the π-π interaction and have a $+0.5e$ charge. Half-charged vertically aligned ET dimers pack into a 2D nearly isotropic triangular network.

One of the ethylene $-C_2H_4-$ groups of each ET molecule are positionally disordered due to strong thermal motion. Therefore, two ET conformations are available. The first, more energetically favorable one is staggered conformation (occupy 75% at room temperature, denoted as **I** in Fig. 1a). The second, less stable one is eclipsed conformation (denoted as **II**).

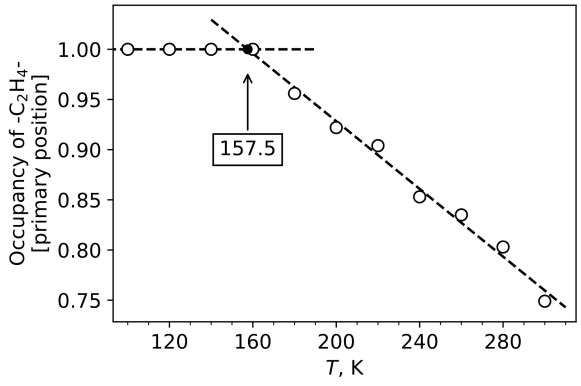

Fig. 2. Temperature behavior of the occupancy of ethylene group the primary position of the ethylene groups $p(T)$

However, $-C_2H_4-$ groups can be frozen by slow cooling down. Plots in Fig. 2 show the temperature dependence of the occupancy p of the primary position **I**. In the high-temperature region, it follows the linear equation with $\partial p/\partial T = -1.7 \cdot 10^{-3}$ K^{-1} and reaches a value of ≈ 1.0 exactly at 157–158 K.

Strictly speaking, it is almost impossible to separate two positions of the ethylene groups below these temperatures. However, a slight amount of ET molecular disorder may still persist. The processes of ordering of terminal $-C_2H_4-$ groups of ET molecules result in several types of order-disorder transitions. For instance, glass-like transitions associated with ethylene group disorder are typical of κ-$(ET)_2X$ and other quasi-two-dimensional ET based salts. The transitions occur at relatively high temperatures, such as $T_g = 70-80$ K in κ-$(ET)_2Cu[N(CN)_2]Cl$, κ-$(ET)_2Cu[N(CN)_2]Br$ and κ-$(ET)_2Cu(NCS)_2$ [21, 22], and $T_{g_1} = 90-100$ K and $T_{g_2} = 120-130$ K in θ-$(ET)_2CsCo(SCN)_4$ and θ-$(ET)_2CsZn(SCN)_4$ salts [23].

3.2. XPS spectra

To reveal the features of the structure of the anionic layer, X-ray photoemission spectroscopy studies were carried out. The typical XPS spectrum of κ-CN crystals and the spectrum of the supporting tape are shown in Fig. 3. The spectra of the samples were recorded within an analysis area of $700 \times 300\,\mu$m^2. According to the XPS spectra, we can conclude that our κ-CN crystals contain copper in +1 and +2 oxidation states. However, because of the limitations the XPS method, it provides an analysis in the few-monolayers-thickness range (≤ 10 nm). However, the concentration of Cu^{2+} inside the crystals may differ from the concentration on their surface.

From the foregoing, the general chemical formula for our κ-CN salt should be κ-$[ET_2]^{2q+}\left[\left(Cu_x^{1+}Cu_{1-x}^{2+}\right)_2(CN)_3\right]^{2q-}$, where q is the charge of the ET molecule and x is the concentration of +1 copper atoms. In copper-pure κ-$[ET_2]^{2q+}\left[\left(Cu^{1+}\right)_2(CN)_3\right]^{2q-}$ cationic $[ET_2]^{2q+}$ layers are charged with $q = 0.5$, which comes from a stoichiometric ratio. The partial substitution $Cu^{1+} \rightarrow Cu^{2+}$ must lead to the discharge of the cationic $[ET_2]^{2q+}$ layer.

The crystal structure of κ-CN crystals potentially contaminated with Cu^{2+} was described and analyzed by H. Yamochi and co-authors using the concept of the

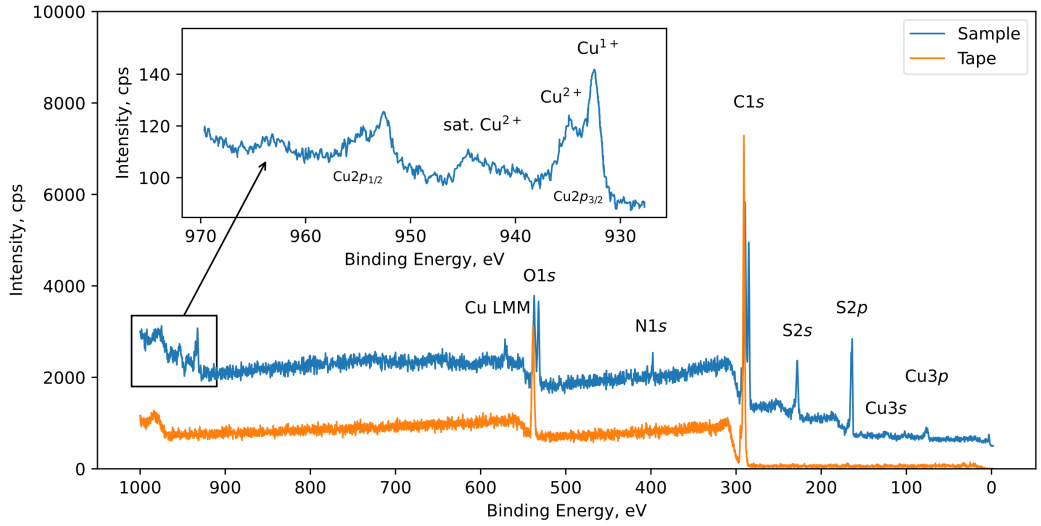

Fig. 3. XPS data for κ-CN crystals

effective volume per conduction electron [24]. The authors discovered that the new phase was metallic at ambient conditions and had a superconducting transition temperature of 3.8 K at ambient pressure. Later, the traces of Cu^{2+} ions were found by using the ESR technique and the spin susceptibility measurements in this kind of κ-CN crystals [25]. According to the reported analysis of magnetometry data, the amount of copper 2+ impurities varies depending on the sample and roughly stands at 88–1200 ppm of total copper atoms. Despite the contamination, a comparative analysis of the structures of all κ-CN phases known at time [26] did not reveal any significant difference in the unit cell parameters or the packing motif between the new κ-CN crystals and those previously reported [3,27]. The authors noted that a qualitative comparison of the fine details of structures cannot be made due to poor-quality data for crystallographic analyses. Although the mechanism of the incorporation of copper 2+ is not entirely clear, it was claimed that some amount of Cu^{1+} may be oxidized into Cu^{2+} during electrocrystallization of κ-CN crystals [25]; in addition, light and water may facilitate the conversion $Cu^{1+} \to Cu^{2+}$ [28].

3.3. Fermi surface and ET charge

In order to find the influence of the average charge of the conductive layers on their electronic structure, we performed a series of DFT calculations of the «isolated» stacked $[ET_2]^{2q+}$ layers in a virtual charge compensation medium. The coordinates of each atom within the $[ET_2]^{2q+}$ layers and their packing motif were taken from the crystal structure data obtained by an X-ray diffraction experiment at 100 K. At this temperature, all parts of the «ET» molecules were completely ordered. The calculations were carried out for several q values ranging from 0.375 to 0.625 in the stable point regime, which means all atomic positions were fixed and the structure was not optimized.

The anionic $Cu_2(CN)_3$ layers were removed from the system; therefore, only cationic layers were considered. Physically, this system corresponds to a periodically stacked $[ET_2]^{2q+}$ 2D layers inserted in a compensating jellium background; thus, the total charge of the system remains neutral. Even though this system has a pure 2D topology, this approximation makes sense since the DFT calculations were based on experimental structure data. In this case, an interlayer interaction was already included because unrelaxed molecular geometries and an unchanged packing motif were used for stable-state calculations.

The calculated Fermi surface of the isolated stacked conductive $[ET_2]^{2q+}$ layers for $q = 0.5$ is shown in Fig. 4 Its shape is typical of 2D organic conductors and consists of two separated parts, namely electron-like sheets and hole-like cylinder, as previously described [3, 25].

Figure 5 shows sections of the Fermi surface of the $[ET_2]^{2q+}$ cation layer by the $(k_y,\ k_z)$ plane for several values of q. According to the DFT calculations, discharge of the layer contributes to the reduction of the volume of the hole-like pockets (α-pockets) that lie between the electron-like sheets (γ-sheets). Squeezing the α-pockets causes the two γ-sheets to become closer within the Brillouin zone and to recede from each other near the zone border. Moreover, the gap between γ and

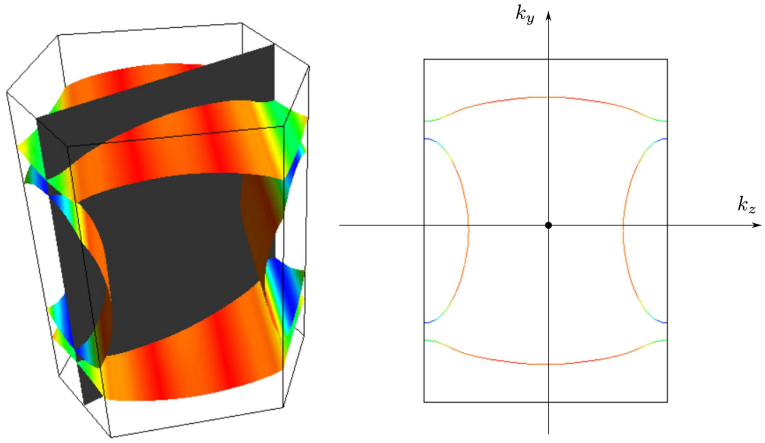

Fig. 4. Fermi surface of the 2D $[ET_2]^{2q+}$ layer within the first Brillouin zone and its projections on the k_y,k_z plane (based on the crystal structure at $T = 100$ K). The surface is colored according to the Fermi velocity, where the transition from blue to red represents a range of approximately 0.09 to 0.18 a.u.

α (denoted as k_{gap} in Fig. 5) tends to be larger when q is small.

The area of the hole α-pocket in the (k_y, k_z) section of k-space (denoted as S_α in Fig. 5) monotonically increases with q (see Fig. 6). This dependence cannot be described as a simple mathematical function, but rather as a combination of linear and exponential functions. It grows linearly at lower charges; however, the growth becomes exponential for charges greater than 0.47. The critical value $q \approx 0.47$ was found by fitting the $S_\alpha(q)$ curve with piecewise combinations of two functions.

To compare the results of the calculations of stacked isolated conductive layers with those of the actual structure containing cationic and anionic layers, we performed calculations of the Fermi surface based on the crystal structure data with the $P2_1$ space group, although the complete structural analysis was carried out using the $P2_1/c$ group. Restriction to the acentric symmetry group is necessary to resolve the structural disorder in the anionic layer. The «full» Fermi surface is quite similar to that calculated for isolated $[ET_2]^{2q+}$ layers except for having smaller k_{gap} (approximately 30% lower) and corrugated electron-like sheets. The uneven charge distribution within the anionic layers results in the formation of symmetric bulges on the sheets toward each other. The gap between the bulges is small in k- and energy spaces (of the order of several meV); therefore, the bulges may easily collapse the thin channel.

It is impossible to adjust the average charge of cationic layers q when the full structure is treated by the DFT calculations since the whole system is already

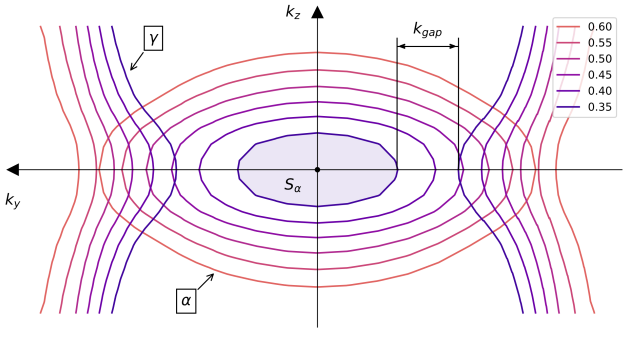

Fig. 5. Sections of the Fermi surface of the stacked $[ET_2]^{2q+}$ cationic layers at several q values (insert in the right upper corner, for clarity, the origin has been shifted to the Brillouin zone boundary)

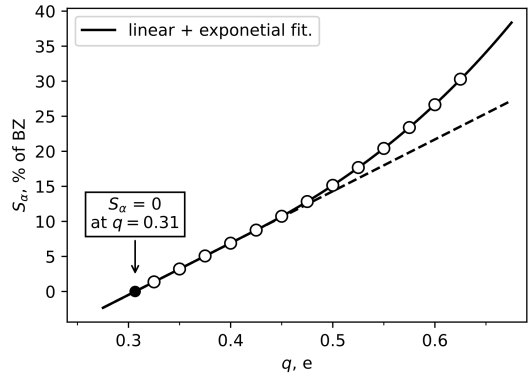

Fig. 6. Area of the (k_y, k_z) section of the hole α-pocket as a percent of the first Brillouin zone

neutral. However, the results obtained for stacked $[ET_2]^{2q+}$ layers in a compensating background can be extrapolated to the case of a full system with alternating cationic and anionic layers.

A decrease in the positive charge of the stacked $[ET_2]^{2q+}$ layered system inevitably leads to an increase of the total energy of the system. In the zero-temperature approximation, the following energy is minimized with the DFT algorithm:

$$E = T_s + J + V + E_{xc}, \quad (1)$$

where T_s is the non-interacting kinetic energy, J is the electron-electron Coulomb energy, V is the potential energy of the electron-nuclei interaction and E_{xc} is the exchange-correlation energy.

However, we performed our calculations in the finite-temperature approximation, which introduces entropy to the system of non-interacting particles. With this kind of calculations, smearing of the Fermi level by the f function is used [29, 30], and the free energy F is minimized. This approximation is usually introduced in the DFT algorithm to improve k-point convergence and has a clear physical interpretation in the case of the Fermi-Dirac (FD) smearing scheme. For FD, F can be written as

$$F = E - \sum \sigma S(f_i), \quad (2)$$

where i is the index of the energy state, $\sigma = k_B T$ is the smearing parameter proportional to the electronic temperature, $S = -[f \cdot \ln(f) + (1-f) \cdot \ln(1-f)]$ is electronic entropy and f is the Fermi-Dirac distribution given by

$$f\left\{\varepsilon_i(\vec{k})\right\} = \frac{1}{e^{\left[\varepsilon_i(\vec{k}) - \bar{\varepsilon}\right]/\sigma} + 1}. \quad (3)$$

In Quantum Espresso (QE) modern smearing technique such as «cold-smearing» are used, which also induce entropy but S can no longer be expressed in terms of f and σ – in terms of T. However, it is still possible to use the QE internal energy parameter E_{demet}, which is negatively proportional to S:

$$E_{\text{demet}} = -\sum_i \sigma S. \quad (4)$$

Electronic entropy S introduced in (4) might be thought of as a small quantitative correction that can be calculated from the band structure [31–33]. It strongly depends on the band structure of the $[ET_2]^{2q+}$ system and reflects the actual electronic structure of impure κ-CN salts because the calculations rely on experimental diffraction data. In particular, S should directly correlate with the density of states at the Fermi level since only these states significantly contribute to the ordering of a statistical collectivity.

Calculated F and E_{demet} energies as a function of $[ET_2]^{2q+}$ charge are shown in Fig. 7. Fitting a parabola to the $E_{\text{demet}}(q)$ data by the least squares method gives the charge $q = 0.488$, at which E_{demet} has a minimum. Considering the general chemical formula κ-$[ET_2]^{2q+}\left[\left(Cu_x^{1+}Cu_{1-x}^{2+}\right)_2(CN)_3\right]^{2q-}$, this average charge corresponds to $x = 0.988$ or 1.2 % substitution positions of Cu^+. In terms of mass concentration of Cu^+, it is approximately 1500 ppm per formula unit, which is close to the values calculated from the Curie constant in the case of some κ-CN crystals [25].

According to equation (4), the minimum of E_{demet} also corresponds to the maximum of the electronic entropy S. This means that from the thermodynamic point of view, the average charge q of the calculated system of isolated $[ET_2]^{2q+}$ layers should be 0.488 as soon as the system reaches an equilibrium state. This value is only 0.022 less than $q = 0.5$ predicted from the X-ray structure analysis without considering cooper impurities. Moreover, it cannot be estimated by the analysis of internal distortions of ET cations i.e., by using Chasseau formula because the accuracy of this technique is 0.1 for high-quality structures [34]. It should be also noted, that optimal charge (0.488) is a feature of this particular system since the calculations were linked to the real non-optimized structure of the crystals examined by the XPS technique. However, we suppose that all our κ-CN samples have some deficiency in the charge of the cationic layers. This q value is slightly larger than that obtained by Raman spectroscopy analysis [35], where ET_2^+ charge disproportionation was found to be disordered and slowly fluctuating. Indeed, such charge fluctuations are definitely connected with external reasons, such as Cu^{2+} impurities.

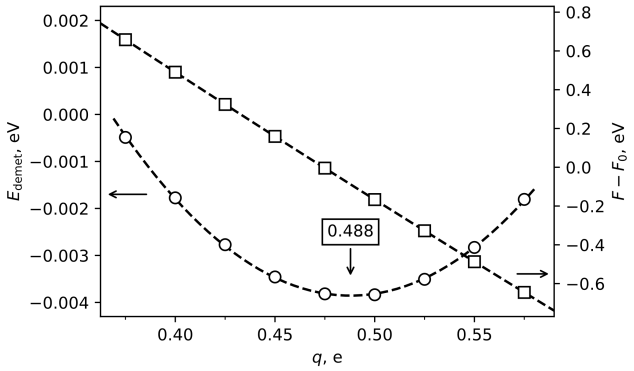

Fig. 7. Shifted total energy $F - F_0$ and E_{demet} energy as a function of ET charge q, $F_0 = -10395.292$ eV

4. CONCLUSIONS

In summary, the single crystals of κ-BEDT--$TTF_2Cu_2(CN)_3$ were studied using multitemperature X-ray diffraction, X-ray photoemission spectroscopy and quantum chemical modelling. X-ray photoemission spectroscopy showed the presence of Cu^{2+} atoms ions in the samples, whereas the analysis of the X-ray diffraction results did not reveal any significant changes in the structure of the κ-CN crystals. This suggests that the impurities were randomly dispersed throughout the polymer layers of the crystals, resulting in charge redistributions in both the cationic and anionic layers and a decrease in the average charge of the conductive layers. The DFT calculations, being based on the unrelaxed real structure, predicted stability of the charge-poor electronic configuration of the cationic layer, and this result is supported by XPS data. The calculations demonstrate that an increase of the concentration of Cu^{2+} impurities in the anionic layer, and, consequently, a decrease in the charge of the cationic layer, modifies the Fermi surface sheets. In particular, energy gaps between separated parts of the Fermi surface are increased, mainly due to shrinking of its hole-like pockets. This «impurity play» may drastically affect the conductive properties of κ-BEDT-$TTF_2Cu_2(CN)_3$ crystals.

Acknowledgements. This work was performed under the state assignment of the Osipian Institute of Solid State Physics, Russian Academy of Sciences (ISSP RAS). Part of this study was carried out using the facilities of the Analytical Center for Collective Use of ISSP RAS and was supported in part through computational resources of HPC facilities at HSE University.

Conflict of interest. The authors declare no conflict of interest.

Author's contributions. The contribution of the authors is equivalent.

REFERENCES

1. G. Saito, T. Enoki, K. Toriumi, and H. Inokuchi, Solid State Commun. **42**, 557 (1982).

2. J.-P. Farges, *Organic Conductors: Fundamentals and Applications*; CRC Press, (1994).

3. U. Geiser, H. H. Wang, K. D. Carlson et al., Inorg. Chem. **30**, 2586 (1991).

4. Y. Shimizu, K. Miyagawa, K. Kanoda et al., Phys. Rev. Lett. **91**, 107001 (2003).

5. H. O. Jeschke, M. de Souza, R. Valenti et al., Phys. Rev. B **85**, 035125 (2012).

6. L. Balents, Nature **464**, 199 (2010).

7. F. L. Pratt, P. J. Baker, S. J. Blundell et al., Nature **471**, 612 (2011).

8. Y. Shimizu, H. Kasahara, T. Furuta et al., Phys. Rev. B **81**, 224508 (2010).

9. S. Elsässer, D. Wu, M. Dressel et al., Phys. Rev. B **86**, 155150 (2012).

10. K. Miyagawa, A. Kawamoto, Y. Nakazawa et al., Phys. Rev. Lett. **75**, 1174 (1995).

11. U. Welp, S. Fleshler, W. K. Kwok et al., Phys. Rev. Lett. **69**, 840 (1992).

12. T. Furukawa, K. Kobashi, Y. Kurosaki et al., Nat. Commun. **9**, 307 (2018).

13. Y. Kurosaki, Y. Shimizu, K. Miyagawa et al., Phys. Rev. Lett. **95**, 177001 (2005).

14. N. Toyota, J. Müller, and M. Lang, *Low-Dimensional Molecular Metals*; Springer, (2007).

15. M. Pinterić, M. Čulo, O. Milat et al., Phys. Rev. B **90**, 195139 (2014).

16. O. Drozdova, G. Saito, H. Yamochi et al., Inorg. Chem. **40**, 3265 (2001).

17. T. Komatsu, T. Nakamura, N. Matsukawa et al., Solid State Commun. **80**, 843 (1991).

18. P. Giannozzi, S. Baroni, N. Bonini et al., J. Phys. Condens. Matter **21**, 395502 (2009).

19. G. M. Sheldrick, Acta Crystallogr. A **71**, 3 (2015).

20. G. M. Sheldrick, Acta Crystallogr. C **71**, 3 (2015).

21. J. Müller, M. Lang, F. Steglich et al., J. Phys. IV **114**, 341 (2004).

22. J. Müller, M. Lang, F. Steglich et al., Phys. Rev. B **65**, 144521 (2002).

23. T. Thomas, Y. Saito, Y. Agarmani et al., arXiv (2021).

24. H. Yamochi, T. Nakamura, T. Komatsu et al., Solid State Commun. **82**, 101 (1992).

25. T. Komatsu, N. Matsukawa, T. Inoue et al., J. Phys. Soc. Jpn. **65**, 1340 (1996).

26. G. C. Papavassiliou, D. J. Lagouvardos, A. Terzis et al., Synth. Met. **61**, 267 (1993).

27. X. Bu, A. Frost-Jensen, R. Allendoerfer et al., Solid State Commun. **79**, 1053 (1991).

28. R. N. Keller, H. D. Wrcoff, L. E. Marchi, Inorg. Synth. **2**, 1 (2007).

29. M. Verstraete, X. Gonze, Phys. Rev. B **65**, 035111 (2001).

30. N. Marzari, *Ab-Initio Molecular Dynamics for Metallic Systems* (1996).

31. F. Zhou, T. Maxisch, and G. Ceder, Phys. Rev. Lett. **97**, 155704 (2006).

32. D. M. C. Nicholson, G. M. Stocks, Y. Wang et al., Phys. Rev. B **50**, 14686 (1994).

33. C. Wolverton and A. Zunger, Phys. Rev. B **52**, 8813 (1995).

34. P. Guionneau, C. J. Kepert, G. Bravic et al., Synth. Met. **86**, 1973 (1997).

35. J. Liebman, K. Miyagawa, K. Kanoda et al., Phys. Rev. B **110**, 165105 (2024).